Bioorganic & Medicinal Chemistry 19 (2011) 789–797

Contents lists available at ScienceDirect

Bioorganic & Medicinal Chemistry

journal homepage: www.elsevier.com/locate/bmc

Studies on 6-chloro-5-(1-naphthyloxy)-2-(trifluoromethyl)-1*H*-benzimidazole/2-hydroxypropyl-β-cyclodextrin association: Characterization, molecular modeling studies, and in vivo anthelminthic activity

Yareli Rojas-Aguirre [a], Lilián Yépez-Mulia [b], Ivan Castillo [c], Fabian López-Vallejo [d], Olivia Soria-Arteche [e], Alicia Hernández-Campos [a], Rafael Castillo [a], Francisco Hernández-Luis [a,*]

[a] Facultad de Química, Departamento de Farmacia, UNAM, México DF 04510, Mexico
[b] Unidad de Investigación Médica en Enfermedades Infecciosas y Parasitarias, IMSS, México DF 06720, Mexico
[c] Instituto de Química, UNAM, Circuito Exterior, Ciudad Universitaria, México DF 04510, Mexico
[d] Torrey Pines Institute for Molecular Studies, 11350 SW Village Parkway, Port St. Lucie, FL 34987, USA
[e] Departamento de Sistemas Biológicos, División Ciencias Biológicas y de la Salud, UAM-X, México DF 04960, Mexico

ARTICLE INFO

Article history:
Received 17 September 2010
Revised 25 November 2010
Accepted 4 December 2010
Available online 9 December 2010

Keywords:
Benzimidazole derivative
Trichinella spiralis
Inclusion complex
HPβCD

ABSTRACT

The purpose of this work is to study the molecular association that occurs between 2-hydroxypropyl-β-cyclodextrin (**HPβCD**) and 6-chloro-5-(1-naphthyloxy)-2-(trifluoromethyl)-1*H*-benzimidazole (**RCB20**), an antiparasitic compound recently found by our research group, with poor aqueous solubility. The complex stability constant and stoichiometric ratio determined by phase-solubility diagram and Job's plot provided evidence that **HPβCD** enhanced water solubility of **RCB20** through inclusion complex formation. Two-dimensional ^{1}H NMR spectroscopy is used to study the molecular arrangement of inclusion complex in solution. These results are further supported using molecular modeling studies. In the solid state, the complexation is confirmed by differential scanning calorimetry, powder X-ray diffraction, and scanning electron microscopy. Finally, **RCB20**/**HPβCD** complex has better activity than **RCB20** against the adult and muscle larvae phase of *Trichinella spiralis*.

1. Introduction

Benzimidazole 2-carbamate derivatives, such as albendazole (**ABZ**) (Fig. 1) and mebendazole (**MBZ**) are widely used in the chemotheraphy of many human and animal enteral helminthic infections.[1] Although **ABZ** has also been used in some tissue-dwelling parasitosis, such as trichinellosis, echinococcis, and neurocysticercosis, high doses and long treatments are required due to the poor solubility and bioavailability of this compound.[2–4] Human trichinellosis, caused by nematodes of the genus Trichinella, has a wide geographical distribution, so far documented in 55 countries around the world, including industrialized and non-industrialized nations.[5–8] It has been estimated that around 11 million people may be infected with the parasite.[9] *Trichinella spiralis*, the main species affecting humans, is mainly acquired by ingestion of raw or undercooked meat contaminated with encysted muscle larvae.[10,11] In addition to its epidemiological relevance, *T. spiralis* can be used as a model for the search of new antiparasitic agents that can be evaluated against both the enteral and systemic phase of the parasites.

In order to identify the potential of the 2-(trifluoromethyl)-1*H*-benzimidazole system as a scaffold for the development of new antiparasitic agents, we have previously synthesized and tested four series of derivatives of this compound.[12–15] These compounds were evaluated in vitro against protozoan parasites (*Giardia intestinalis, Entamoeba histolytica, and Trichomonas vaginalis*) and the helminth *T. spiralis*. One of these derivatives, 6-chloro-5-(1-naphthyloxy)-2-(trifluoromethyl)-1*H*-benzimidazole, in this work named **RCB20** (Fig. 1), presented an antiparasitic profile similar to **ABZ**,[15] but not present in its structure a group of easy biological oxidation as thioester of albendazole, therefore is not expected to present a extensive first-pass metabolism. However, in these studies **RCB20**

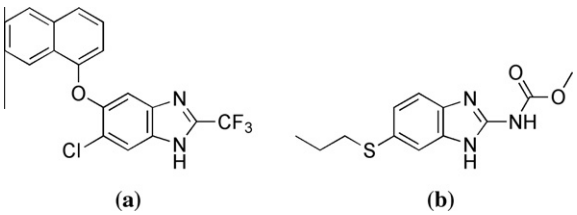

Figure 1. (a) 6-Chloro-5-(1-naphthyloxy)-2-(trifluoromethyl)-1*H*-benzimidazole (**RCB20**); (b) methyl[5-(propylthio)-1-*H*-benzimidazol-2-yl]carbamate (**ABZ**).

* Corresponding author. Tel./fax: +52 56225287.
E-mail address: franher@unam.mx (F. Hernández-Luis).

0968-0896/$ - see front matter © 2010 Elsevier Ltd. All rights reserved.
doi:10.1016/j.bmc.2010.12.015

showed poor aqueous solubility, which hampered the subsequent in vivo experimental trials. Although poor aqueous solubility is ideal for luminal infections, it represents a problem in the treatment of systemic helminthiasis such as trichinellosis. Furthermore, the lack of water solubility reduces flexibility for drug formulation and administration. To overcome these drawbacks, increasing the aqueous solubility of **RCB20** is an important goal. An alternative to increase the solubility, stability, and bioavailability of drugs has been the formation of inclusion complexes with cyclodextrins (CDs).[16,17] These cyclic oligomers are formed by glucopyranose molecules bound through 1–4 bonds, and are most commonly composed by 6 (α-CD), 7 (β-CD) or 8 (δ-CD) glucose units. CDs are able to form inclusion complexes with different classes of molecules, modifying their physical, chemical and biological properties. The hydrophobic cavity of CDs can form inclusion systems with a variety of guest molecules. The binding is governed by the molecular polarity and ability to closely fit within the cavity.[18,19] Among CDs, 2-hydroxypropyl-β-cyclodextrin (**HPβCD**) appears to be especially useful based on its low toxicity, complexation potential, and great water solubility.[20,21]

The aim of this work was to study the molecular association that takes place between **RCB20** and **HPβCD**. To ascertain the inclusion complex formation, phase-solubility diagram and Job's plot were performed. The inclusion mode was estimated by two-dimensional proton nuclear magnetic resonance (2D ^{1}H NMR) spectroscopy and molecular modeling. Additionally, differential scanning calorimetry (DSC), powder X-ray diffraction (XRD), and scanning electron microscopy (SEM) were employed to characterize the complex in solid state. Finally, the in vivo anthelminthic activity against *T. spiralis* of the **RCB20**/**HPβCD** system was evaluated.

2. Results and discussion

2.1. Chemistry

The benzimidazole derivative **RCB20** was prepared according to our published procedure with minor modifications.[15] Briefly, 4,5-dichloro-2-nitroaniline was subjected to an aromatic nucleophilic substitution reaction with 1-naphthol under known conditions, and the ether obtained was reduced with hydrogen and Raney-Nickel. The corresponding 1,2-phenylenediamine formed was immediately condensed with trifluoroacetic acid to give **RCB20**. The compound was purified by recrystallization from cyclohexane, and its structure, established by spectroscopic and spectrometric methods, was consistent with that previously reported.[15]

2.2. Phase-solubility diagram

As shown in Figure 2, there is a linear increase in **RCB20** solubility with increasing concentrations of **HPβCD** indicating the formation of a soluble complex between **RCB20** and this CD. The solubility curve obtained can be classified as A_L type.[22] Because such profile was characterized by a slope of less than 1, it was assumed that the solubility increase was due to the formation of a 1:1 complex.[22] The apparent stability constant ($K_{1:1}$) was estimated from the straight line of the phase-solubility diagram according to the equation: $K_{1:1} = m/So(1-m)$, where m is the slope of the linear plot and So is **RCB20** intrinsic water solubility (So = 11 mg/L, 30.32 μM) determined by UV-spectroscopy.[23] Inclusion complex aqueous solubility was also evaluated.[23] Solubility value obtained of 15 mg/L represents a 36% increase relative to free **RCB20**.

The value of $K_{1:1}$ is a useful index to estimate the degree of binding strength of the complex. Values of $K_{1:1}$ have been reported in 0–10,000 M^{-1} range. Constants values less than 100 M^{-1} denote weak guest–host associations, whereas values near to 10,000 M^{-1} indicate strong interactions.[4,16,24–26] The $K_{1:1}$ value for the **RCB20**/HPβCD inclusion complex was 5157 M^{-1}, suggesting that a favorable interaction between them occurs.

2.3. Stoichiometry determination by the continuous variation method (Job's plot)

The Job's method (Fig. 3) was used for the determination of the stoichiometry of the inclusion complex from UV-spectrophotometric measurements.[24] The plot shows a maximum value at r = 0.5 and a symmetrical shape, indicating the existence of a complex with a 1:1 stoichiometry. This result is in agreement with the phase-solubility studies between **RCB20** and **HPβCD**.

2.4. ^{1}H NMR spectroscopy

In order to observe the inclusion mode of **RCB20** into **HPβCD**, a NMR study was performed. The inclusion of one molecule in aqueous CD solution can be evidenced by modifications of the 1D ^{1}H NMR spectra of guest and host molecules.[27] However, in this case, the NMR study was inadequate to allow the full spectroscopic characterization of the complex in D_2O, particularly by the continuous variation method necessary to establish the degree of association between **RCB20** and **HPβCD** in aqueous solution. Nonetheless, ^{1}H NMR spectra of **RCB20**, **HPβCD,** and **RCB20**/**HPβCD** were acquired in MeOD/D_2O mixtures. The maximum amount of deuterated water that could be employed without precipitation of **HPβCD** and the inclusion complex corresponded to 70:30 ratio (Fig. 4). The singlets arising from H-3$_{\mathbf{HP\beta CD}}$ and H-5$_{\mathbf{HP\beta CD}}$ in a MeOD/D_2O solution of **HPβCD** resonate at δ 4.013 and 3.882 ppm, respectively. In the inclusion complex, the corresponding signals shift to δ 4.025 and 3.892 ppm ($\Delta\delta$ = 0.012 and 0.010 ppm). The shift of the resonances is consistent with inclusion of **RCB20** in the hydrophobic cavity of the cyclodextrin. Both H-3 and H-5 are situated in the inner part of

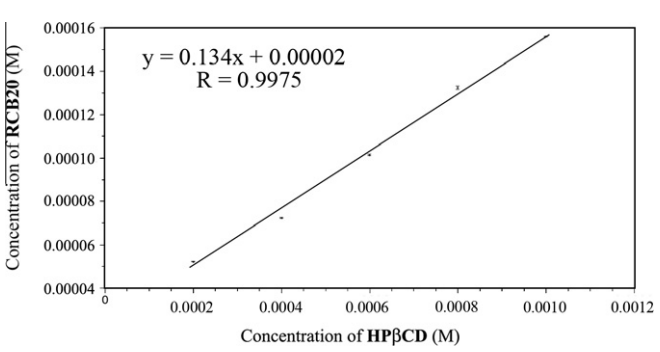

Figure 2. Phase-solubility diagram for **RCB20**/**HPβCD** host–guest system at 25 °C.

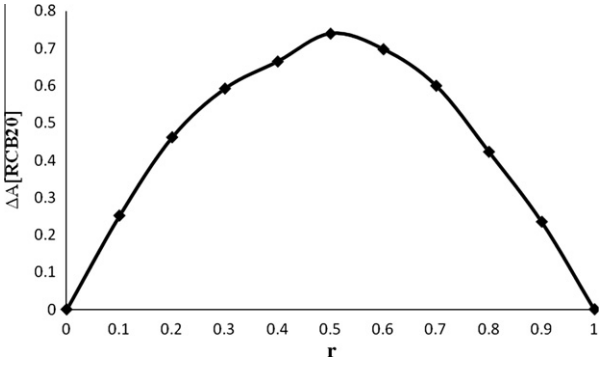

Figure 3. Continuous variation plot of the **RCB20**/**HPβCD** system.

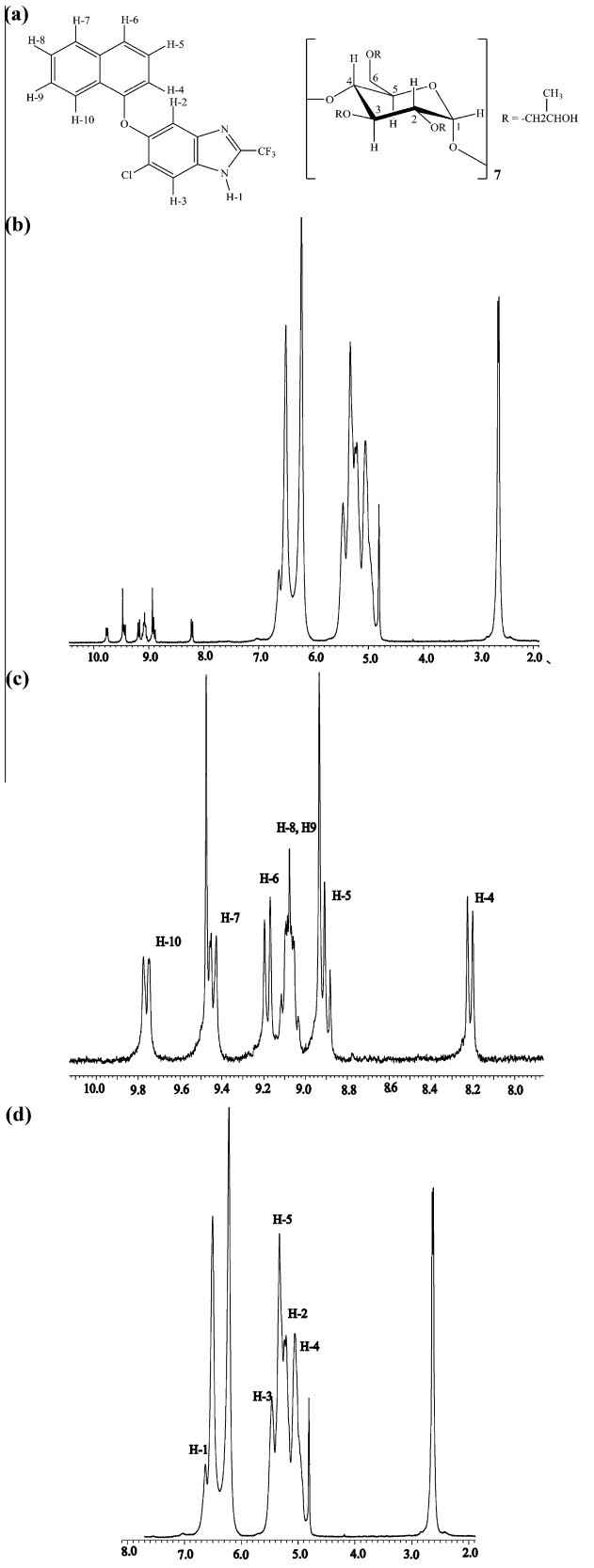

Figure 4. (a) Identification of **RCB20** and **HPβCD** protons; (b) ^{1}H NMR spectrum of the **RCB20**/**HPβCD** inclusion complex in MeOD/D_2O (70:30); (c) ^{1}H NMR spectrum of **RCB20** in MeOD/D_2O (90:10); (d) ^{1}H NMR spectrum of **HPβCD** in MeOD/D_2O (70:30).

Table 1
Chemical shifts of 9 mM solutions of free **HPβCD** and **RCB20**/**HPβCD** inclusion complex (MeOD/D_2O 70:30).

Assignment	δ^a (free compound)	δ^a (complex)	$\Delta\delta$ (complex free)
H-$1_{\mathbf{HP\beta CD}}$	5.185	5.192	0.007
H-$2_{\mathbf{HP\beta CD}}$	3.775	3.774	0.001
H-$3_{\mathbf{HP\beta CD}}$	4.013	4.025	0.012
H-$4_{\mathbf{HP\beta CD}}$	3.614	3.621	0.010
H-$5_{\mathbf{HP\beta CD}}$	3.882	3.892	0.010

[a] δ, ppm.

the **HPβCD**, wherein H-3 is on the wide side and H-5 is on the narrow side of the cavity.[19] Thus, the data shown in Table 1 indicate that **RCB20** is being included into the cavity from the wide side. In the case of the benzimidazole derivative **RCB20**, ^{1}H NMR spectra were acquired in 90:10 MeOD/D_2O to ensure complete dissolution of the compound. Some of the resonances of **RCB20** also shifted upon complex formation, from δ 7.955 (H-$7_{\mathbf{RCB20}}$) and 7.404 (H-$5_{\mathbf{RCB20}}$) in the free compound to δ 8.001 and 7.475 ppm. Although the displacement of the signals could be attributed to the inclusion of the naphthyl moiety of **RCB20** into the hydrophobic cavity of **HPβCD**, it is important to note that the use of different solvent systems (90:10 vs 70:30 MeOD/D_2O) must also influence the observed chemical shifts.

The information on the spatial proximity of the molecules in the inclusion complex was confirmed by two-dimensional rotating-frame NOE spectroscopy (ROESY).[27,28] For this purpose, 2D ROESY spectra of the isolated 1:2 **RCB20**/**HPβCD** complex were acquired in the same MeOD/D_2O (70:30) solvent mixture; although the stoichiometry of the inclusion complex was determined to be 1:1, ROESY spectra have been determined in the presence of excess cyclodextrin.[29] The contour plot revealed that two signals of **RCB20** (H-7 and H-5 at δ 8.001 and 7.475 ppm, respectively) have intense intermolecular cross-peaks with H-3 cyclodextrin proton (Fig. 5). In addition, the peaks at δ 7.745 and 7.639 ppm, corresponding to H-6 and H-8 of **RCB20** have weak intermolecular interactions with H-3 of **HPβCD**.

According to the ROESY studies, the strongest interactions correspond to H-$3_{\mathbf{HP\beta CD}}$–H-$7_{\mathbf{RCB20}}$ and to a lesser extent with H-$5_{\mathbf{RCB20}}$; the interactions H-$5_{\mathbf{HP\beta CD}}$–H-$5_{\mathbf{RCB20}}$ and H-$5_{\mathbf{HP\beta CD}}$–H-$7_{\mathbf{RCB20}}$ are very weak. Additionally, it can also be seen that H-$3_{\mathbf{HP\beta CD}}$ interacts with H-4, H-6, H-8 and H-9 of **RCB20** but not in a strong manner. The latter reveals that **RCB20** was not completely inserted into **HPβCD** cavity. It is not surprising that the most probable insertion mode of **RCB20** involves the naphthyl moiety, since it represents the most hydrophobic part of the molecule (Fig. 6). All these observations reinforce the inclusion mode proposed according to ^{1}H NMR (Table 1).

2.5. Molecular modeling

In order to extend the information obtained from NMR results described above, molecular dynamics simulation studies were carried out. Figure 7a shows a plot of the total energy (kcal/mol) versus simulation time (ns); it is clear from this plot that during the entire trajectory the total energy remained almost constant, implying a reasonable stability for the **RCB20**/**HPβCD** complex. Figure 7b–d show the plots for the distance in Å of H-7 of **RCB20** and different H-3 of **HPβCD** (i.e., H-$7_{\mathbf{RCB20}}$–H-$3_{\mathbf{HP\beta CD}}$) versus simulation time (ns). In general, Figure 7b–d show the distances for six out of the seven H-3 hydrogen atoms of **HPβCD**—red and blue colors indicate any out of two H-3 hydrogen atoms separated by two glucopyranoside units. For instance, as can be seen in

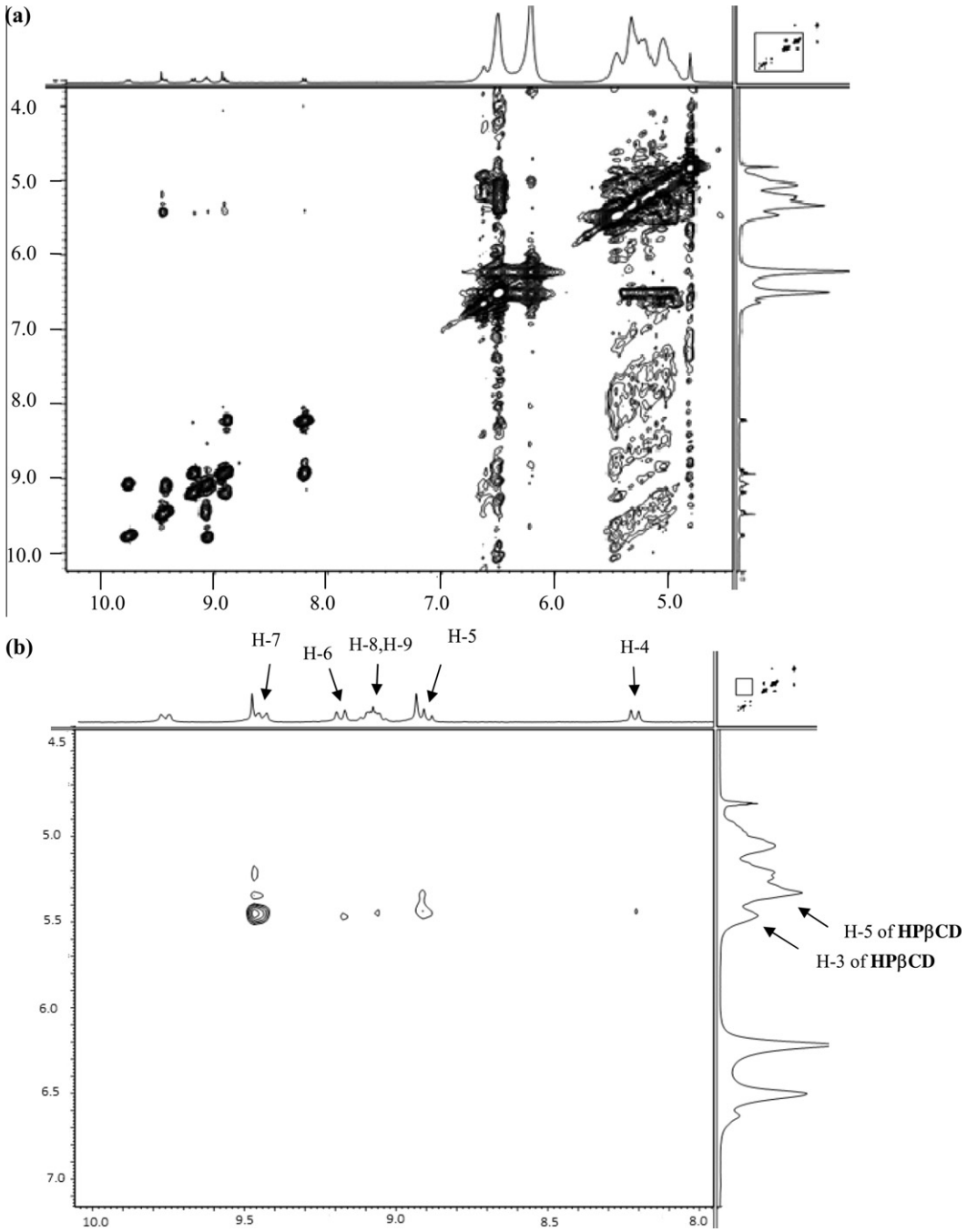

Figure 5. (a) ROESY spectrum partial contour of a solution of **RCB20**/**HPβCD** 1:2 complex (15 mM) in MeOD/D_2O (70:30); (b) ROESY spectrum expansion showing the cross-peaks between the aromatic signals of **RCB20** and **HPβCD** protons.

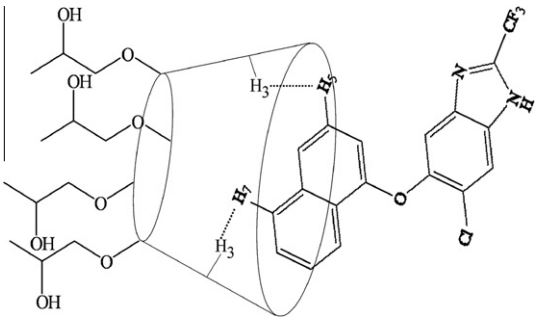

Figure 6. Insertion mode of **RCB20** into **HPβCD** cavity.

Figure 7c, during the first 0.7 ns of simulation, H-7 of **RCB20** is kept in close proximity to H-3_1 (blue) and far from H-3_4 (red); during the remainder of the simulation time (0.8 ns), H-7 is now close to H-3_4 and far from H-3_1. Similar conclusions can be obtained from Figure 7b, analyzing the distances during the simulation time between H-7–H-3_2 (red) and H-7–H-3_5 (blue) or from Figure 7d between H-7–H-3_7 (red) and H-7–H-3_3 (blue).

From Figures 7b–d, it can be concluded that **RCB20** seems to be rotating along the trajectory inside the cavity of the host, since throughout the first 0.7 ns, H-7 remains very close to one of the H-3 hydrogen atoms of **HPβCD** (e.g., H-3_1), with an average distance (H-$7_{\mathbf{RCB20}}$–H-$3_{\mathbf{HP\beta CD}}$) of 3.01 Å. During the rest of the trajectory, it shifts towards the opposite H-3 (e.g., H-3_4, two

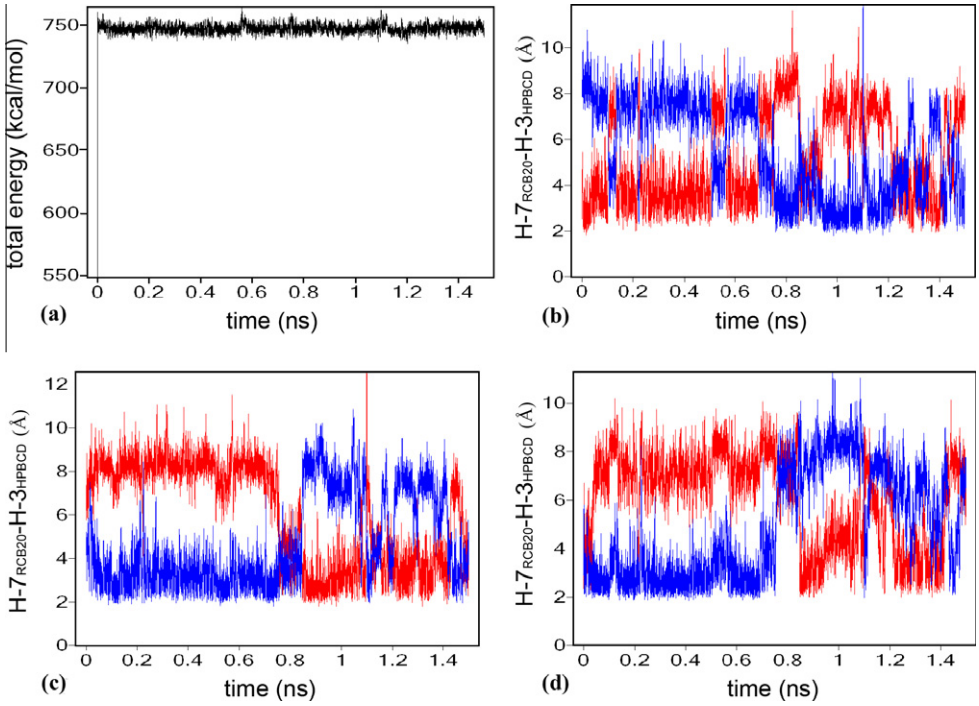

Figure 7. Molecular dynamics simulation. (a) Total energy versus simulation time; (b–d) distance between different H-3 hydrogen atoms into **HPβCD** cavity and H-7 of **RCB20** versus simulation time.

glucopyranoside units away) within **HPβCD** cavity, while maintaining an average distance (H-$7_{\mathbf{RCB20}}$–H-$3_{\mathbf{HP\beta CD}}$) of 3.91 Å (Fig. 7c).

In order to get a representative structure of the complex, an average structure was obtained during a simulation range of 0.1–0.6 ns, with almost constant (H-$7_{\mathbf{RCB20}}$–H-$3_{\mathbf{HP\beta CD}}$) distance. Figure 8 shows the average distance (H-$7_{\mathbf{RCB20}}$–H-$3_{\mathbf{HP\beta CD}}$) between H-7 and two of its nearest H-3 hydrogen atoms within the host cavity, with distances of 2.543 and 2.940 Å, respectively.

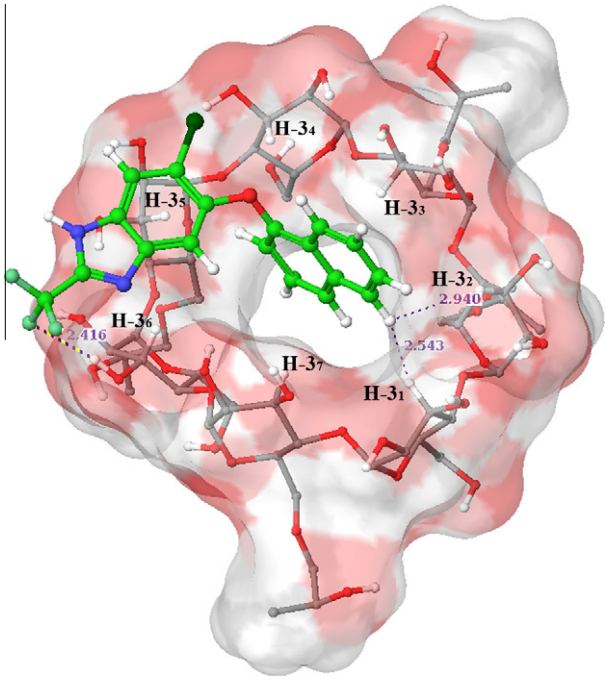

Figure 8. Representative averaged and optimized structure of **RCB20**/**HPβCD** inclusion complex obtained during 0.5 ns of dynamics simulation (range 0.1–0.6 ns).

Interestingly, the molecular dynamics simulation showed that the **RCB20**/**HPβCD** inclusion complex can be stabilized by attractive short contacts between the hydrogen atoms of the **HPβCD** hydroxyl groups at C-4 positions, and the fluorine atom of the trifluoromethyl group, at C-2 of **RCB20**. The O–H···F-C distance of the average structure was 2.416 Å (Fig. 8). It is noteworthy that this distance is shorter than the sum of the van der Waals radii (H···F = 2.67 Å) with an angle O–H···F = 169.8°, and it might be considered a weak hydrogen bond.[30]

2.6. Differential scanning calorimetry

DSC curves obtained from the isolated host and guest, along with physical mixture and the inclusion complex are presented in Figure 9. **RCB20** (Fig. 9a) exhibited two endothermic peaks corresponding to melting point (107 °C), characteristic of a crystalline material, and compound decomposition (184 °C). **HPβCD** (Fig. 9b) showed two broad endotherms (60 °C and 218 °C), the first assigned to loss of water, and the second one to thermal decomposition.[31] In the physical mixture (Fig. 9c) the melting peak of **RCB20** was retained at 107 °C indicating the absence of any interactions with the cyclodextrin; the peak reduction in intensity is due to molar components relationship (**RCB20**/**HPβCD**, 1:2). The inclusion complex (Fig. 9d) shows a broad endothermic peak in the range of 50–100 °C due to loss of water molecules, which are likely hydrogen-bonded to the cyclodextrin OH groups, outside the hydrophobic cavity.[32,33] In addition, the disappearance of **RCB20** melting endotherm is a strong indication of inclusion complex formation.

2.7. X-ray diffraction analysis

Powder X-ray diffraction (XRD) scattering represents a useful technique for the detection of cyclodextrin inclusion complexes.[34,35] Thus, further information on **RCB20**/**HPβCD** complex formation was obtained by wide angle XRD scattering.[36] The diffractograms of pure samples of **HPβCD** and **RCB20** (Fig. 10), the physical

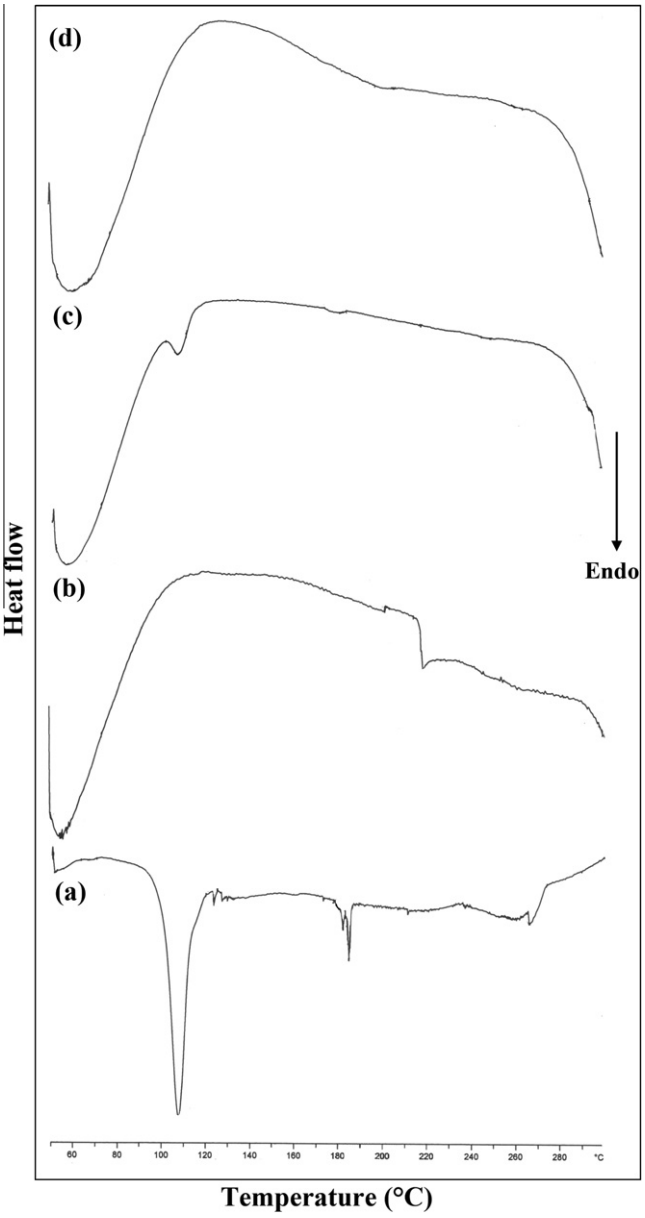

Figure 9. DSC curves: (a) **RCB20**, (b) **HPβCD**, (c) **RCB20**/**HPβCD** physical mixture, (d) **RCB20**/**HPβCD** inclusion complex.

mixture of the two components, and the inclusion complex clearly reveal differences between the pure substances and the final inclusion complex obtained. The diffraction pattern of **RCB20** powder (Fig. 10a) revealed several sharp high intensity peaks suggesting that the compound is present in a crystalline phase, in contrast to the amorphous character of **HPβCD** (Fig. 10b).[27,28,33] The diffraction pattern of the physical mixture (Fig. 10d) confirmed that it contains the respective individual components, but with some changes in the intensity of several peaks of this sample as compared to **RCB20** diffractogram. The XRD pattern of the inclusion complex (Fig. 10c) did not display the characteristic peaks of **RCB20** and the observed amorphous halo is indicative of the transformation of **RCB20** from crystalline to amorphous state. The above observations are indicative of the inclusion of **RCB20** into the cavity of amorphous **HPβCD**.

2.8. Scanning electron microscopy

SEM analysis was performed to investigate the morphology of pure materials and the changes produced on it by the formation

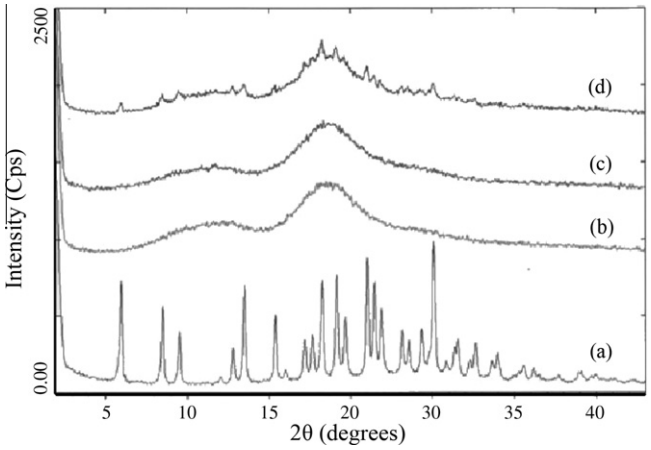

Figure 10. Powder X-ray diffractograms (Cu-κα): (a) **RCB20**, (b) **HPβCD**, (c) **RCB20**/**HPβCD** inclusion complex, (d) **RCB20**/**HPβCD** physical mixture.

of the inclusion complex. Figure 11 illustrates the SEM micrographs of pure materials, the physical mixture and inclusion complex **RCB20**/**HPβCD** at 500 magnifications, which were used for shape and surface morphology. **RCB20** (Fig. 11a) appears in the micrograph as needle-like crystals, in agreement with the sharp peaks observed by powder XRD. In contrast, **HPβCD** (Fig. 11b) is seen as amorphous pieces of quasi-spherical particles.[36,37] In the physical mixture comparable morphology with pure materials of **RCB20** and **HPβCD** can be observed (Fig. 11c). **RCB20** characteristic crystals and **HPβCD** particles are clearly visible in the micrograph, indicating the absence of host–guest interactions. Finally, the inclusion complex (Fig. 11d) appears in the form of irregular particles of variable sizes, in which the original morphologies of **RCB20** and **HPβCD** have disappeared.

2.9. Biological assays

The biological activity of **RCB20**/**HPβCD** inclusion complex and **RCB20** was evaluated against the adult worm and muscle larva of *T. spiralis* in a murine model of trichinellosis. **ABZ** and **ABZ**/**HPβCD** inclusion complex were also included. Animals infected but not treated were included as negative control. All the compounds were tested at equimolar doses of 11 mg/kg of **ABZ**. Number adult/mouse and number of muscle larvae/mouse are presented in Table 2. **RCB20**/**HPβCD** inclusion complex was the most active against *T. spiralis* adult, reducing the parasite load by 41%, and proved to be more active than **RCB20** alone (32%). However, **RCB20**/**HPβCD** inclusion complex reduced just 14% the systemic phase of *T. spiralis*. The activity of **ABZ** and **ABZ**/**HPβCD** at the enteral level was comparable to **RCB20** alone, and **RCB20**/**HPβCD**, respectively. Nevertheless, **ABZ** and **ABZ**/**HPβCD** showed slightly higher activity against *T. spiralis* muscle larvae.

3. Conclusion

The molecular association type of **RCB20** and **HPβCD** was determined. Phase-solubility profile indicated that **HPβCD** enhanced water solubility of **RCB20** through inclusion complex formation. The NMR and molecular modeling studies reveal that in this complex, **RCB20** is held within the lipophilic cavity of **HPβCD** by its naphthyl fragment. Results obtained by DSC, XRD and SEM support the complex formation in solid phase. **RCB20**/**HPβCD** inclusion complex showed better activity against *T. spiralis* adult worms than **RCB20** alone. The efficacy of the inclusion complex against the muscle larvae stage was better than **RCB20** alone but it did not surpass **ABZ** efficacy. The complex formation of **RCB20** with **HPβCD**

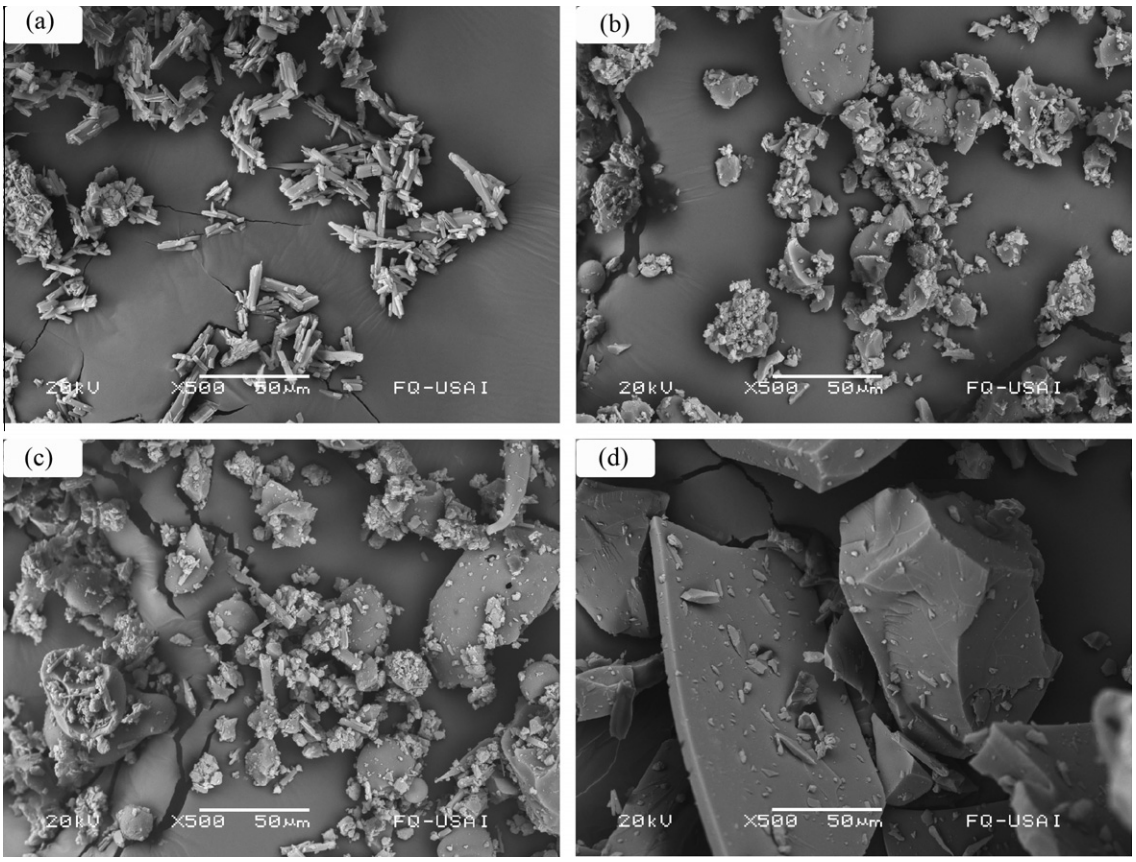

Figure 11. SEM: (a) **RCB20**, (b) **HPβCD**, (c) **RCB20**/**HPβCD** physical mixture (1:2), (d) **RCB20**/**HPβCD** inclusion complex (1:2).

Table 2
In vivo activity of **RCB20**, **ABZ**, and their inclusion complexes with **HPβCD** against the adult worm and muscle larvae of *T. spiralis*

Compound	Adults/mouse[a] (mean ± SD)	Muscle larvae/mouse[b] (mean ± SD)
Control	467 ± 167	310,000 ± 12,172
RCB20	323 ± 114[c]	291,450 ± 5586[c]
RCB20/**HPβCD**	270 ± 73[c]	264,650 ± 16829[c]
ABZ	353 ± 171[c]	260,500 ± 28284[d]
ABZ/**HPβCD**	290 ± 90[c]	233,375 ± 25632[d]

[a] Groups of six mice were infected with 500 *T. spiralis* ML and treated at day 3 post-infection (pi) with a single dose of the drugs. Animals were sacrificed at day 6 pi, and adults were obtained as previously described.[3]

[b] Groups of 10 mice were infected with 500 *T. spiralis* ML and treated with the drugs at day 28 pi for seven consecutive days. Animals were sacrificed on day 7 after treatment, and ML were obtained as previously described.[3] Two independent experiments were performed.

[c] $p \pm 0.05$.

[d] $p \pm 0.05$.

resulted in better antiparasitic efficacy at intestinal level, however for systemic infection treatment, new drug delivery strategies need to be developed.

4. Experimental

4.1. Materials

Synthetic starting material, **ABZ** and **HPβCD** (MW = 1380) with an average degree of molar substitution of 0.6, were purchased from Aldrich Chemical Co. Other reagents and chemicals were of analytical reagent grade. All experiments were carried out using ultrapure water (MILLI Q).

4.2. Preparation of the inclusion complex

The inclusion complex was obtained by dissolving **RCB20** and **HPβCD** at a 1:2 molar ratio in an ethanol–water solution (25:75 v/v). The resulting mixture was stirred at 25 °C for 7 days protected from light to prevent degradation. After this period, the solution was subjected to evaporation at 40 °C and under vacuum for the resulting solid inclusion complex to be collected. A physical mixture was also prepared to test for possible inclusion by thoroughly mixing **RCB20** and **HPβCD** in the same molar ratio (1:2) in a mortar for 5 min. Although 1:1 stoichiometry was obtained from phase-solubility measurements, for production, an excess of cyclodextrin was employed to increase the yield of complexation. The efficiency of complexation may sometimes be rather low, and therefore relative large amounts of cyclodextrin must be used to complex small amounts of drug.[38,39]

4.3. Phase-solubility diagram

The solubility studies were carried out according to the method of Higuchi and Connors.[22] A fivefold molar excess of **RCB20—relative** to the highest concentrated **HPβCD solution—was** added to **HPβCD** solutions of increasing concentrations (0.0002, 0.0004, 0.0006, 0.0008, and 0.001 M). The mixtures were stirred for 48 h at room temperature protected from light. After this period the amount of **RCB20** in solution was determined after filtration through a 0.2 μm Millipore filter using a UV spectrophotometer at 290 nm. This experiment was repeated three times.

4.4. Stoichiometry determination by the continuous variation method (Job's plot)

The stoichiometry of inclusion was determined by the continuous variation technique (Job's method).[40] The plot was determined from UV-spectrophotometric measurements in water at 25 °C at 290 nm. The total molar concentration of the two species, **RCB20** and **HPβCD**, was kept constant (0.2 mM), and their mole fractions varied from 0.1 to 0.9.

4.5. Solid phase characterization of inclusion complex

Thermal analyses (differential scanning calorimetry-DSC) of the pure materials (**RCB20**, **HPβCD**), the physical mixture and the inclusion complex were recorded on a Mettler Toledo DSC 821^e with 5 °C/min heating rate and under 100 mL/min N_2 flow. Powder X-ray diffraction (XRD) was measured in a Siemens Dn 5000 diffractometer using Cu-κα (λ = 1.5406 Å) with 30 mA, 35 kV and scanning rate of 1 °C/min. The scanning electron microscopy (SEM) was performed to the raw materials and to the inclusion complex using the Jeol JSM 5900 LV apparatus, after samples had been gold sputtered. The parameters used were SEI mode, samples height less than 5 mm; voltage of 20 kV; work distance 11 mm and spot size of 22. Specific adjustments of focus, brightness and contrast were performed.

4.6. ^{1}H NMR spectroscopy

^{1}H NMR spectra were acquired on a JEOL Eclipse 300 spectrometer at 300 MHz; the samples were referenced relative to the residual peak of MeOD at δ ppm.

4.7. Molecular modeling

Due to the difficulty associated with the structural description of chemically-modified cyclodextrins, there is a degree of uncertainty in the substitution pattern of **HPβCD**. Since our experimental work involved **HPβCD** with a degree of substitution of 0.6, four 2-hydroxypropyl groups were added at O-6 positions; this approach has been successfully applied in previous studies.[41,42] Structures of **HPβCD** and **RCB20** were built using the sketch molecule module of the SYBYL 7.3 package (Tripos Co., USA). The host and guest structures were individually optimized by MMFF94 force field using the conjugate gradient method, and a convergence criterion of 0.005 kcal/mol. The AUTODOCK 4.0 software was used to obtain a **RCB20**/**HPβCD** complex with a suitable geometry as starting point to carry out a molecular dynamics simulation.[43] The Lamarckian genetic algorithm was employed to generate a total population of 100 complexes. An initial population of 100 individuals with a maximal number of energy evaluations of 2,500,000 and a maximal number of generations of 50,000 were the parameters used for the global search. The results were clustered into groups with root mean square deviations (RMSDs) <1.0 Å. A grid box of 70 × 70 × 70 points was used to calculate the energy maps. The points were separated from each other by 0.375 Å. The selected complex to carry out molecular dynamics simulation was that with the highest score, and with the naphthyl ring inserted into the **HPβCD** cavity from wider side of the rim, in agreement with the results obtained by NMR spectroscopy.

The molecular dynamics simulation was carried out during 1.5 ns to verify the stability of the complex. Periodic boundary conditions were used during the simulation. An isothermal–isobaric (NPT) ensemble and a time step of 1.0 fs were employed, maintaining the temperature at 300 K, and a pressure of 1.0 atm. A nonbonded cutoff (8.0) and dielectric constant of 32.6 were used as an approach to the methanol/water mixture used in the NMR studies. The system was initially equilibrated for 100 ps. Intermediate structures were saved every 50 fs for analysis. A representative structure of the **RCB20**/**HPβCD** complex was obtained averaging the trajectory within a range of 0.1–0.6 ns.

4.9. Antitrichinellosis activity

Groups of 10 BALB/c mice were experimentally infected by intragastric route with 500 *T. spiralis* muscle larvae suspended in 0.1 mL of 0.2% bactoagar. **RCB20** and **RCB20**/HPβCD were freshly prepared in cremophor/ethanol/water (80:10:10). For comparison, groups of *T. spiralis* infected mice treated with **ABZ** and **ABZ**/**HPβCD** were also included. Compounds were administered orally at equimolar doses of 11 mg/kg of **ABZ**. In order to evaluate their activity against the adult worm of *T. spiralis*, they were orally administered at day 3 post-infection (pi) and parasites were obtained from the intestine of treated animals at day 6 pi and counted according to the method previously described.[3] Two independent experiments were performed. The statistical significance of data obtained was determined by One way ANOVA test and Dunnett *t* test.

The activity of **RCB20** and **ABZ** and their respective inclusion complex with **HPβCD** was also evaluated against *T. spiralis* muscle larvae. For this, groups of 10 BALB/c mice were experimentally infected as previously indicated and treated with the compounds and their inclusion complexes at day 28 pi for seven consecutive days with an equimolar dose of 11 mg/kg of **ABZ**. Muscle larvae were obtained by artificial counted seven days after the last administration.[3] The mean of adult worms and standard deviation obtained in each group was included in Table 2. The statistical significance of data obtained was determined by One way ANOVA test and Dunnett *t* test.

Animal experiments were performed according to Norma Oficial Mexicana (NOM-062-Z00-1999) published on August 22, 2009.

Acknowledgments

We are grateful to Margarita Guzmán, Marisela Gutiérrez, Cecilia Salcedo and Iván Puente from Facultad de Química, USAI, UNAM, for the determination of DSC thermograms, IR spectra, powder X-ray diffractograms and SEM micrographs, respectively. We also thank Dr. José L. Medina-Franco for discussion about molecular modeling and Jesús Azucena for his assistance during the in vivo experiments. This study was supported by grants from PAPIIT-UNAM IN210809, CONACyT 80093.

Supplementary data

Supplementary data associated with this article can be found, in the online version, at doi:10.1016/j.bmc.2010.12.015.

References and notes

1. Sharma, S. *Adv. Drug Res.* **1994**, *25*, 105.
2. Jung, H.; Medina, L.; García, L.; Fuentes, I.; Moreno, R. *J. Pharm. Pharmacol.* **1998**, *50*, 43.
3. Yépez-Mulia, L.; Morales-Hurtado, R.; Viveros-Guzmán, N.; Cedillo, R.; Hernández-Luis, F.; Castillo, R.; Hernández, A.; Muñoz, O. *Arch. Med. Res.* **1999**, *30*, 368.
4. Evrard, B.; Chiap, P.; De Tullio, P.; Ghalmi, F.; Piel, G.; Van Hees, T.; Crommen, J.; Losson, B.; Delattre, L. *J. Controlled Release* **2002**, *85*, 45.
5. Gajadhar, A.; Gamble, H. *Vet. Parasitol.* **2000**, *93*, 183.
6. Pozio, E.; Hoberg, E.; La Rosa, G.; Zarlenga, D. *Inf. Gen. Evol.* **2009**, *9*, 606.
7. Pozio, E.; Murrell, K. *Adv. Parasitol.* **2006**, *63*, 367.
8. Pozio, E. *Vet. Parasitol.* **2007**, *149*, 3.
9. Dupouy-Camet, J. *Vet. Parasitol.* **2000**, *93*, 191.
10. Pozio, E.; Murrell, K. *Int. J. Parasitol.* **2000**, *30*, 1339.
11. Gajadhar, A.; Pozio, E.; Gamble, H.; Nöckler, K.; Maddox-Hyttel, C.; Forbes, L.; Vallée, I.; Rossi, P.; Marinculić, A.; Boireau, P. *Vet. Parasitol.* **2009**, *159*, 197.

12. Navarrete-Vázquez, G.; Cedillo, R.; Hernández, A.; Yépez, L.; Hernández-Luis, F.; Valdéz, J.; Morales, R.; Cortés, R.; Hernández, M.; Castillo, R. *Bioorg. Med. Chem. Lett.* **2001**, *11*, 187.
13. Navarrete-Vázquez, G.; Yépez-Mulia, L.; Hernández-Campos, A.; Tapia, A.; Hernández-Luis, F.; Cedillo, R.; González, J.; Martínez-Fernández, A.; Martínez-Grueiro, M.; Castillo, R. *Bioorg. Med. Chem.* **2003**, *11*, 4615.
14. Navarrete-Vázquez, G.; Rojano-Vilchis, M.; Yépez-Mulia, L.; Meléndez, V.; Gerena, L.; Hernández-Campos, A.; Castillo, R.; Hernández-Luis, F. *Eur. J. Med. Chem.* **2006**, *41*, 135.
15. Hernández-Luis, F.; Hernández-Campos, A.; Castillo, R.; Navarrete-Vázquez, G.; Soria-Arteche, O.; Hernández-Hernández, M.; Yépez-Mulia, L. *Eur. J. Med. Chem.* **2010**, *45*, 3135.
16. Loftsson, T.; Hreinsdóttir, D.; Másson, M. *Int. J. Pharm.* **2005**, *302*, 18.
17. Tong, W.; Wen, H. In *Water-insoluble Drug Formulation*; Liu, R., Ed.; CRC Press, 2008; pp 146–154.
18. Connors, K. *Chem. Rev.* **1997**, *97*, 1325.
19. Uekama, K.; Hirayama, F.; Arima, H. In *Cyclodextrins and Their Complexes*; Dodziuk, H., Ed.; Wiley-VCH, 2006; pp 381–396.
20. Brewster, M.; Loftsson, T. *Adv. Drug Delivery Rev.* **2007**, *59*, 645.
21. Loftsson, T.; Duchêne, D. *Int. J. Pharm.* **2007**, *329*, 1.
22. Higuchi, T.; Connors, K. *Adv. Anal. Chem. Instrum.* **1965**, *4*, 117.
23. Baka, E.; Comer, J.; Takács-Novák, K. *J. Pharm. Biomed. Anal.* **2008**, *46*, 335.
24. Stella, V.; Venkatramana, M.; Rao, E.; Zannou, A. *Adv. Drug Delivery Rev.* **1999**, *36*, 3.
25. Pérez-Cruz, F.; Jullian, C.; Rodríguez, J.; Arán, V.; Olea-Azar, C. *Bioorg. Med. Chem.* **2009**, *17*, 4604.
26. Crupi, V.; Ficarra, R.; Guardo, M.; Majolino, D.; Stancanelli, R.; Venuti, V. *J. Pharm. Biomed. Anal.* **2007**, *44*, 110.
27. Yang, B.; Lin, J.; Chen, Y.; Liu, Y. *Bioorg. Med. Chem.* **2009**, *17*, 6311.
28. Gaspar de Araújo, M. V.; Barbosa Vieira, E. K.; Lázaro, G. S.; Conegero, L. S.; Pastor Ferreira, O.; Almeida, L. E.; Barreto, L. S.; Bezerra da Costa, N., Jr.; Gimeneza, I. F. *Bioorg. Med. Chem.* **2007**, *15*, 5752.
29. Cruz, J. R.; Becker, B. A.; Morris, K. F.; Larive, C. K. *Magn. Reson. Chem.* **2008**, *46*, 838.
30. Carosati, E.; Sciabola, S.; Cruciani, G. *J. Med. Chem.* **2004**, *47*, 5114.
31. Veiga, V.; Merino, M.; Fernández, D.; Lozano, R. *J. Therm. Anal. Calorim.* **2002**, *68*, 511.
32. Fini, A.; Ospitali, F.; Zoppetti, G.; Puppini, N. *Pharm. Res.* **2008**, *25*, 2030.
33. Zoppetti, G.; Puppini, N.; Ospitali, F.; Fini, A. *J. Pharm. Sci.* **2007**, *96*, 1729.
34. Ribeiro, L.; Loftsson, T.; Ferreira, D.; Veiga, F. *Chem. Pharm. Bull.* **2003**, *51*, 914.
35. Zingone, G.; Rubessa, F. *Int. J. Pharm.* **2004**, *291*, 3.
36. Badr-Eldin, S. M.; Elkheshen, S. A.; Ghorab, M. M. *Eur. J. Pharm. Biopharm.* **2008**, *70*, 819.
37. de Araujo, D. R.; Tsuneda, S. S.; Cereda, C. M. S.; Carvalho, F. D. G. F.; Preté, P. S. C.; Fernandes, S. A.; Yokaichiya, F.; Franco, M. K. K. D.; Mazzaro, I.; Fraceto, L. F.; Braga, A. F. A.; de Paula, E. *Eur. J. Pharm. Sci.* **2008**, *33*, 60.
38. Tommasini, S.; Calabr'o, M. L.; Stancanelli, R.; Donato, P.; Costa, C.; Catania, S.; Villari, V.; Ficarra, P.; Ficarra, R. *J. Pharm. Biomed. Anal.* **2005**, *39*, 572.
39. Loftsson, T.; Masson, M.; Sigurjonsdottir, J. F. *Pharm. Sci.* **1999**, *9*, 237.
40. Job, P. *Ann. Chim.* **1928**, *9*, 113.
41. Yap, K. L.; Liu, X.; Thenmozhiyal, J. C.; Ho, P. C. *Eur. J. Pharm. Sci.* **2005**, *25*, 49.
42. Mura, P.; Bettinetti, G.; Melani, F.; Manderioli, A. *Eur. J. Pharm. Sci.* **1995**, *3*, 347.
43. Morris, G. M.; Goodsell, D. S.; Halliday, R. S.; Huey, R.; Hart, W. E.; Belew, R. K.; Olson, A. J. *J. Comput. Chem.* **1998**, *19*, 1639.